POLYMERS FOR ADVANCED TECHNOLOGIES
Polym. Adv. Technol. 2008; **19**: 588–595
Published online 2 May 2008 in Wiley InterScience (www.interscience.wiley.com) DOI: 10.1002/pat.1111

PAT

Flammability reduction of flexible polyurethane foams via carbon nanofiber network formation

Mauro Zammarano[1*,†], Roland H. Krämer[2], Richard Harris, Jr.[1], Thomas J. Ohlemiller[1], John R. Shields[1], Sameer S. Rahatekar[1], Silvia Lacerda[3] and Jeffrey W. Gilman[1]

[1]Building and Fire Research Laboratory, National Institute of Standards and Technology (NIST), 100 Bureau Drive, Gaithersburg, MD 20899-8665, USA
[2]School of Chemical Science and Engineering, Fibre and Polymer Technology, Royal Institute of Technology, SE-100 44 Stockholm, Sweden
[3]Polymer Division, NIST, Gaithersburg, MD 20899, USA

Received 11 February 2008; Accepted 12 February 2008

Untreated polyurethane flexible foams (PUFs) are prone to rapid fire growth due to their low density and low thermal conductivity. Furthermore, the low viscosity of the decomposition products generates severe dripping that increases the fire hazard related to the combustion of PUFs. In fact, this downward flow of flaming liquid often results in a pool-fire that promotes flame propagation and boosts the rate of heat release (HRR) due to a significant increase in the burning area and to feed-back between the flame on the pool-fire and the residual foam. In this work the effect of nanoparticles, i.e., clays and carbon nanofibers (CNFs), on the HRR is investigated with special attention given to melt dripping. A modified cone calorimeter test has been developed for this purpose. It is shown that CNFs form an entangled fiber network which eliminates melt dripping and decreases the HRR. Published in 2008 by John Wiley & Sons, Ltd.

KEYWORDS: nanocomposite; polyurethane; flammability; foam

INTRODUCTION

Addition of a nanoadditive to a polymer can create significantly more interfacial area and filler–filler interactions than in conventional composites. Above a critical concentration extended particle–particle interactions can lead to the formation of a jammed network structure that increases the viscosity of the liquid phase generated during the thermal degradation of most polymers. The material as a whole will behave rheologically like a gel.[1] This phenomenon improves the flame resistance by decreasing the release rate of combustible gases emitted by bubbling and by creating an insulating protective shield on the surface of the polymer.[2,3] In this work it is shown that a percolated network of nanoparticles in PUFs may act as a super-structure that prevents foam collapse, melt dripping, and pool-fire formation; this limits flame spread, by preventing the transfer of burning material to adjacent surfaces, and results in a reduced HRR.

*Correspondence to: M. Zammarano, BFRL, NIST, 100 Bureau Drive, Gaithersburg MD 20899–8665, USA.
E-mail: zammarano@gmail.com
†NIST Guest Researcher from CimtecLab, Area Science Park, Padriciano 99, 34012 Trieste, Italy.

EXPERIMENTAL PART

Materials

All foams were derived from a standard formulation for flexible slabstock foams based on a glycerol propoxylate-block-ethoxylate polyol (Voranol 235-056, Dow) and toluene diisocyanate (TDI, a 80:20 molar mixture of 2,4 and 2,6 toluene diisocyanate, Mondur TD80, Bayer). The following additives were used: amine catalyst (type AC1, Dabco 33 LV, Air Products or type AC2, Niax A-1, GE silicones), tin catalyst (stannous octoate, Aldrich), brominated-phosphorous flame retardant blend (Br-P FR) (Firemaster 550, Great Lakes), silicone surfactant (Dabco DC 5943, Air Products), cell opener (type CO1, Ortegol 501, Degussa, or type CO2, Voranol CP 1421, Dow), coupling agent (LICA38, Kenrich), and blowing agent (methylene chloride, Mallinckrodt). The standard formulation (Control) containing Br-P FR was modified as shown in Table 1 by substituting 62% by mass of the Br-P FR with one of the following: oxidized carbon nanofibers (CNF) (Pyrograph III, Grade PR 24-PS OX, Applied Sciences Inc), micron-sized talc (Baker), or organo-modified montmorillonite clay (OMC) (Cloisite 30B, Southern Clay Products). For all composite foams, the amount of the inorganic filler, regardless of surface treatments, amounted to 3.9% by mass. The fillers were dried

Table 1. Foam formulations*

	Control	Talc	CNF	Clay
Polyol	58.84	58.72	58.38	56.27
TDI	30.31	30.25	30.04	28.99
Br-P FR	6.24	2.35	2.33	2.25
Talc	—	3.88	—	—
CNFs	—	—	3.85	—
OMC	—	—	—	4.94
DI water	2.24	2.23	2.22	2.14
AC1	0.12	0.12	0.12	0.17
AC2	—	—	0.12	—
Tin catalyst	0.14	0.34	0.53	0.32
Surfactant	0.59	0.59	0.44	0.42
Blowing agent	1.53	1.53	1.52	1.46
CO1	—	—	0.29	—
CO2	—	—	—	2.81
Coupling agent	—	—	0.15	0.22

*Concentrations are expressed in % mass.

(vacuum, 12 hr, 80°C) before dispersion in the polyol. Dispersions were performed in a colloid mill (Rimek, Karnavati) operating at 366 rad sec^{-1} for 15 min by adding first the coupling agent (when required) and then the solid filler. Foams were prepared by charging all components except TDI into a polypropylene beaker, premixing at 50 rad sec^{-1} for 10 sec, adding TDI, stirring the solution for 5 sec at 50 rad sec^{-1}, and pouring the product into a cylindrical cardboard container.

Methods

Optical micrographs were acquired on an inverted microscope (Nikon Eclipse TE300). To enable imaging, the colloid mill dispersions were diluted with untreated polyol. Thermogravimetric measurements were obtained with a thermogravimetric analyzer (TGA Q500, TA Instruments) by heating small foam samples (4 mg) on a platinum pan in nitrogen or technical air (heating rate of 5°C min^{-1}) to 600°C. A laboratory-scale small-angle X-ray scattering (SAXS) instrument, employing Mo $K\alpha_1$ radiation ($\lambda = 0.07093$ nm) at 17.44 keV, was used for monitoring the d-spacing in the clay nanocomposites.[4] SEM micrographs were acquired on a S-4700 Hitachi microscope at an accelerating voltage of 20,000 V. Laser scattering (Horiba LA-950) was used for analyzing particle size distribution. Rheological data were collected using an AR G2 (TA instruments) rheometer using a parallel plate set up with 780 μm gap. Frequency sweep tests were performed at 0.5% strain. For shear viscosity tests all samples were pre-sheared at 100 sec^{-1} for 30 sec and then equilibrated for 2 min at 25°C.

The flammability of the foams was investigated by a modified cone calorimeter that measures the HRR while taking into account dripping effects and the heat feedback due to the formation of a pool-fire. Further details on the test are given in the remainder of the paper.

The absorption of polyol on the residues from the modified cone test was measured. About 0.02 g of residue were placed on a paper filter (42.5 mm diameter, qualitative grade, Whatman) and gently dipped in polyol for 5 min. The excess of polyol was removed in three steps by placing the filter on adsorbing paper (the adsorbing paper was replaced between each step): first at room temperature for 30 min, then at 80°C for 30 min, and finally for 3 hr at 80°C. The net absorption of polyol was calculated by subtracting from the gross polyol absorption, the average absorption of polyol measured for the paper filter alone. The values of polyol absorption reported here are the averages of five measurements on different samples. The reported uncertainties are calculated according to the law of propagation of error by combining the individual standard uncertainties for the absorption on the filters and residues.[5]

The contact angles between the polyol and OMC or CNF films were measured with a Kruss G2 goniometer by static sessile drop method. OMC and CNF films were prepared by sonicating the additive (0.3 g) in methanol (50 ml) for 15 min, filtering, and then pressing (about 2 MPa) the filtrate at room temperature between two kapton films. The contact angles were recorded with a high-resolution camera right after the polyol drop touched the film. The contact angles reported here are the averages of 12 measurements.

RESULTS AND DISCUSSION

Characterization of the polyol-filler dispersions

SAXS data (Fig. 1) for OMC with polyol after dispersion in the colloid mill, and the OMC in the final foam showed a d-spacing of 3.8 nm and 4.0 nm, respectively. The d-spacing for pristine OMC was 1.8 nm.[6] This increase of clay d-spacing in the liquid dispersion and in the OMC foam indicates the formation of a nanocomposite with an intercalated morphology.[7]

Laser scattering was used to further characterize the dispersion of OMC in polyol. The sample was diluted by adding polyol in order to optimize the signal. The estimated aggregate size of OMC in polyol was 100 μm at a concentration of about 1% by mass of additive. Thus, OMC is intercalated by the polyol but the dispersion is not homogeneous.

Such heterogeneity (aggregated clusters) was confirmed by optical microscopy (OM). The particle dispersion in diluted samples containing 0.1% by mass of additive in the

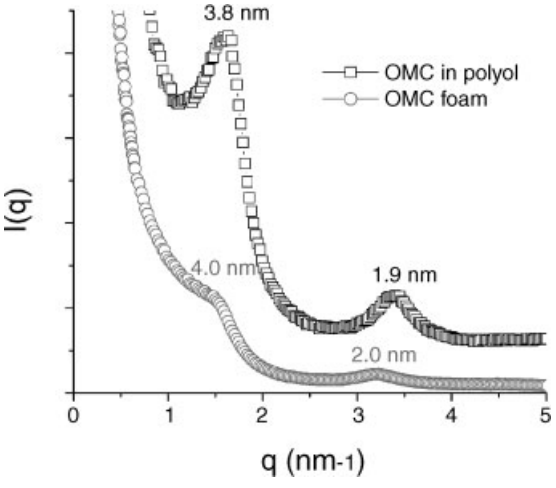

Figure 1. SAXS data for the OMC-containing samples after dispersion in polyol and after foaming. This figure is available in color online at www.interscience.wiley.com/journal/pat

DOI: 10.1002/pat

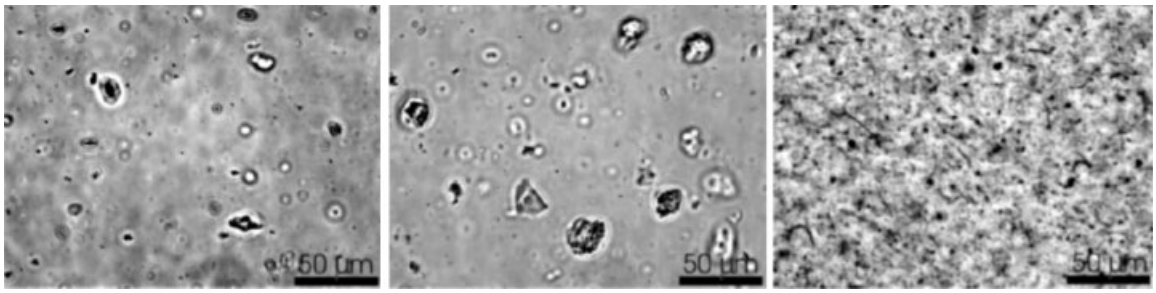

Figure 2. Optical micrographs of the dispersions containing 0.1% by mass of talc (left), clay (middle), and carbon-nanofibers (right) in the polyether polyol after mixing in the colloid mill.

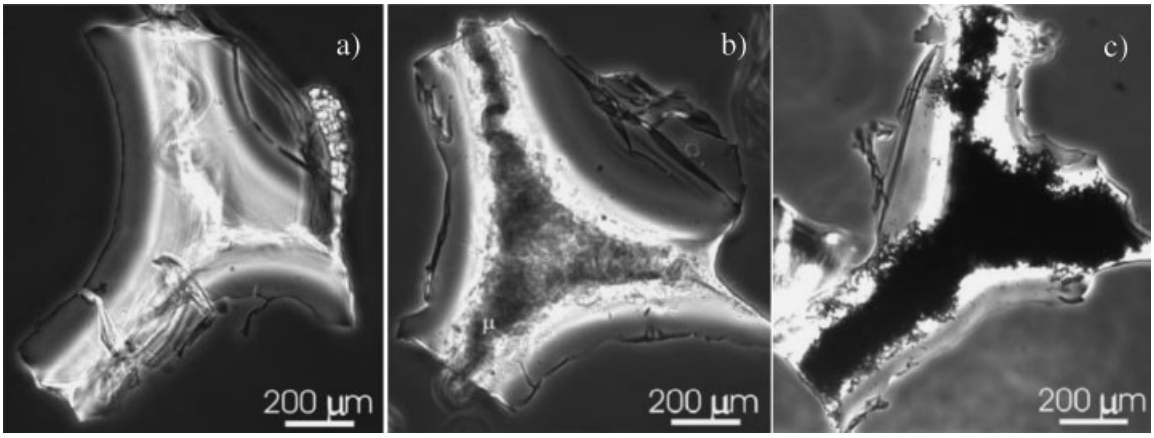

Figure 3. Optical micrographs of small samples cut from the control foam (a), OMC composites (b), and CNF composite (c).

polyol was observed by OM (Fig. 2). The clay dispersion (Fig. 2, middle) contained particles from 10 to 20 µm and smaller ones less than 5 µm; all particles are presumably aggregates of multi-layer stacks. The talc dispersion (Fig. 2, left) had particles from 2 to 10 µm. OM of the CNF/polyol (Fig. 2, right) showed the most homogeneous dispersion with individual fibers, which were 10–40 µm long, and 1–2 µm amorphous carbon particles. Occasionally, larger particles 10–20 µm were found; only very few of those were agglomerates of nanofibers.

Foam characterization

The density of the talc, CNF, and clay composite foam samples was $(28.0 \pm 0.1)\,\mathrm{kg\,m^{-3}}$, $(27.3 \pm 0.2)\,\mathrm{kg\,m^{-3}}$, and $(27.5 \pm 0.2)\,\mathrm{kg\,m^{-3}}$, respectively. Similar densities were achieved by tuning the amount of catalysts (see Table 1).

Imaging of the foam by flat-bed scanner (not shown) revealed a higher tendency towards closed cells for the clay nanocomposites, and to a lesser extent for the CNF composites, relative to the control or talc composite foams; thus variations in airflow values are expected between the three composite foams.

OM revealed that the particle concentration was much higher in the center of the cell strut than in the outer parts of it. This can be seen most clearly for the CNF foams (Fig. 3). In addition, the cell membranes were almost devoid of particles. The area of higher particle concentration formed a continuous network throughout the foam that was interrupted only in a few spots. Hence during foaming, a transition occurred from the initially homogenous distribution of the CNFs (Fig. 2c) into a structure of enriched and depleted domains (Fig. 3c). Very similar results were found for the clay composites. The question arises as to how this biphasic structure is formed. The most likely process is that the nanoparticles diffuse from the cell membrane towards the meniscus (strut) during the initial period of the foam rise when temperature is high and gelling has not yet occurred.[8] Such a process is commonly observed for particles in liquid films.[9,10] Cell opening leads to a rupture of the thin cell walls and to some extent to the flow of material from the cell wall to the strut.[11] Thereby, the struts are coated with material of lower particle concentration. This biphasic core-skin structure is extremely interesting because it causes a local increase of the nanoparticle concentration in the core of the foam struts. As a result, a percolated network can be achieved with a lower nanoparticle concentration.

Thermal stability of foams

TGA data in nitrogen for the Talc, OMC, and CNF foams are shown in Fig. 4. No relevant difference in terms of onset decomposition temperature or mass loss rate can be observed between the three composites. The urethane and urea bonds in PUFs decompose at a significant rate above 200 °C to regenerate the liquid precursors, i.e., polyols and isocyanate, without producing much volatile material.[12] For flexible-TDI-based foams, most of the TDI will volatilize quickly below 300°C, leaving a mixture of regenerated polyol and a few per cent of nitrogen based compounds; further decomposition leads to the formation of a limited amount of char containing thermally stable moieties like carbodiimides

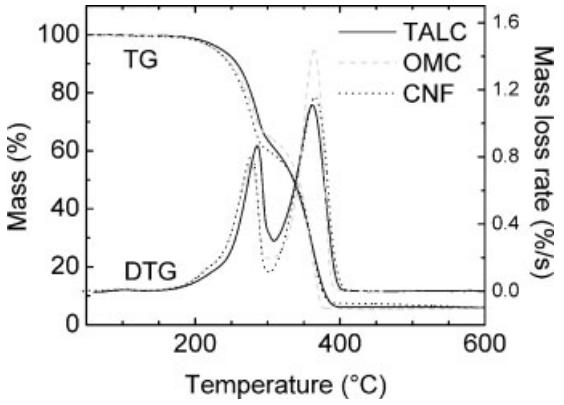

Figure 4. TGA in nitrogen for the talc, C30B, and CNFs foams. This figure is available in color online at www.interscience.wiley.com/journal/pat

and isocyanurate rings.[13] The TGA in Fig. 4 shows a two-step process. The first-stage weight loss at 280°C is about 28%. Supposing that this weight loss consists of solely TDI used in the foam (about 30%), then more than 90% of TDI volatilizes during the first step of decomposition. The second step is associated with the volatilization of the regenerated polyol. The total residue at 550°C of the formulations containing inorganic fillers was 5–7% by mass for all the formulations. The residue for the neat polyurethane foam without any additive was between 1 and 2% by mass; thus, it appears that no significant char enhancement was induced by the presence of the fillers in the composite foams once the inorganic content is taken into account. Similar results were observed also in air (not shown).

Rheology of the filler-polyol dispersions

The rheology of the filler-polyol mixtures can be used to estimate the rheological behavior of the melt produced by the thermal degradation of the foam. As mentioned before, this melt is mostly formed by regenerated polyol. Fig. 5 shows the viscosities for the neat polyol, and the dispersions containing talc, CNF, and OMC that were used for foaming. Note that the filler concentration in the dispersions is different. It is 6.2% by mass for talc and CNF, and 8.0% by mass for OMC. This is to keep a constant inorganic fraction of the filler for all composite foams. The CNF and OMC dispersions also contain the coupling agent (4% by mass of additive).

CNFs induce a two-orders-of-magnitude increase in low-shear viscosity (η) as compared to the neat polyol, whereas η is only slightly affected by the presence of micro-dispersed talc or intercalated OMC. This can be explained by the differences in terms of aspect ratio and inter-particle attractive energy between the fillers.[14,15] In spite of the intercalation of the clay that increases the apparent volume fraction of the additive, at low shear and in the presence of the coupling agent, the OMC generates a lower viscosity than talc. However, as shown in Fig. 6, for the mixtures without the coupling agent (OMC no C.A.) the low-shear-rate viscosity of the clay containing dispersion increases by four orders of magnitude. Thus, the coupling agent drastically decreases η most likely by reducing the inter-particle attractive energy between the micro-aggregates

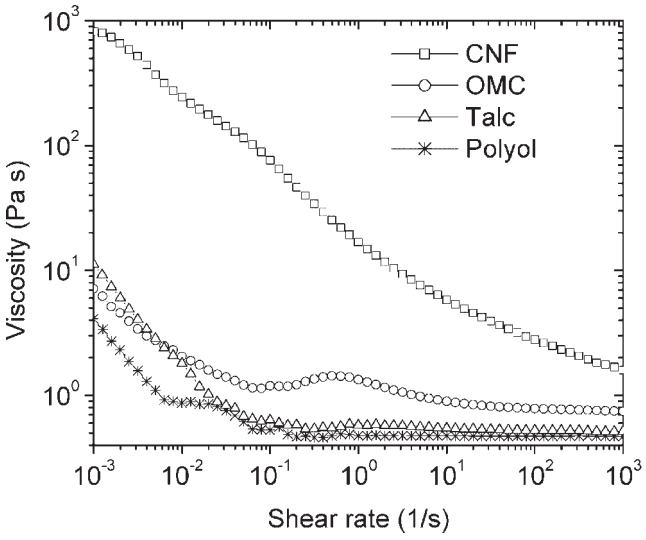

Figure 5. Shear viscosity tests for the neat polyol and the polyol dispersions containing 6.2% by mass of CNF or talc, or 8.0% by mass of OMC. The CNF and OMC dispersions contain also the coupling agent (4% by mass of additive).

of intercalated clay tactoids. The use of the coupling agent with OMC was necessary to reduce the viscosity and make the dispersion foamable. This same coupling agent had a negligible effect on the viscosity of the CNF dispersion (not shown); however, it was used in both the CNF and the clay foam in order to exclude that any potential difference in terms of fire performance between the two foams might be due to the coupling agent.

Figure 6 also shows the viscosity of the OMC dispersions with the coupling agent annealed in air at 300°C for 10 min (OMC-300°C), or at 350°C for 10 min (OMC-350°C). The mass loss during the annealing was 1.9% and 15.2% by mass for OMC-300°C and OMC-350°C, respectively. OMC-300°C

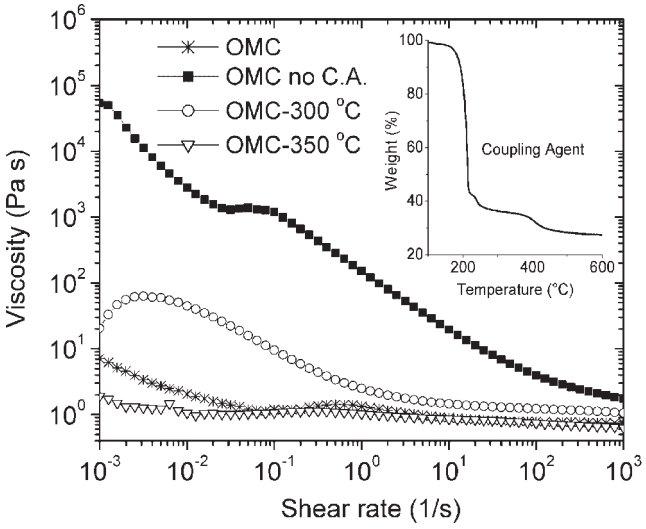

Figure 6. Shear viscosity tests for the polyol dispersions containing OMC without coupling agent (OMC no C.A.); with coupling agent (OMC); with coupling agent and annealing at 300°C (OMC-300°C); and with coupling agent and annealing at 350°C (OMC-350°C). In the inset the TGA in nitrogen of the coupling agent is shown.

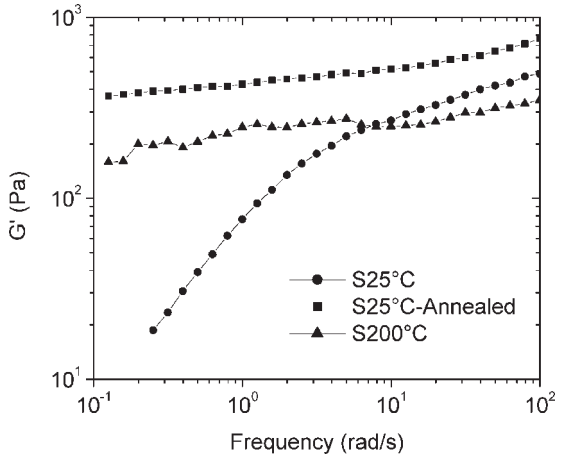

Figure 7. Frequency sweep test for the CNF dispersion with coupling agent measured at the following conditions: room temperature (S25°C); room temperature after 10 min annealing at 200°C (S25°C–Annealed); 200°C (S200°C).

shows an increase in viscosity especially at low shear that might be due to the decomposition of the coupling agent (see the inset of Fig. 6). Note that at 300°C the first step of foam decomposition is complete and that the liquid polyol is regenerated. One might think that the coupling agent can be profitably used to decrease the viscosity at low temperature, thus allowing foaming, and yet restore a high viscosity during thermal degradation, thereby helping prevent melt-drip formation during burning. This is only partially true because a further increase in temperature, up to 350°C, causes a drastic drop in the low-shear viscosity that is likely due to the polyol decomposition and the collapse of the intercalated structure by decomposition of the clay surfactant.[16]

Figure 7 shows the frequency sweep tests for the CNF-polyol dispersions with the coupling agent at different temperatures and preconditioning: at room temperature (S25°C); at room temperature after 10 min annealing at 200°C (S25°C–Annealed); at 200°C (S200°C). The S25°C sample has the same rheological response observed in a Newtonian liquid, i.e., $G' \propto \omega^2$ (where G′ and ω are the elastic modulus and the oscillatory frequency, respectively) at low frequency. However, for S25°C–Annealed and S200°C, G′ became nearly constant at low frequency. This indicates that by controlling the temperature or the thermal history it is possible to induce a transition from a liquid-like to solid-like behavior. This solid-like behavior is due to the formation of a mechanically stable network of CNFs.[17] It was reported that an increase in temperature might induce a spatial rearrangement of the nanoparticles and generate a percolated network.[18] The proper control of this liquid–solid transition allows one to get foamable formulations at lower temperature and rigid-like behavior at higher temperature; this transition might be thermally activated during the exothermic foaming process and/or thermal degradation.

Flammability

During horizontal cone calorimeter tests of PUF, a significant problem arises; a reduction in the incident heat flux occurs due to the receding surface of the collapsing foam.[19,20] Furthermore, the liquefied flaming material produced during the test is retained in the sample holder, whereas, in a real fire scenario it may spread out increasing the burning surface area and the HRR. A modified cone calorimeter test has been developed which comes closer to the real-life scenario, since it measures the HRR while taking into account dripping effects and the heat feedback due to the formation of a pool-fire. The experimental configuration (Fig. 8a, b) consists of a foam specimen (95 mm × 85 mm × 40 mm) held in a wire frame 20 mm above a catch pan (100 mm × 60 mm aluminum pan on a 2 mm thick insulating ceramic felt) which collects the melt from the specimen. During the test, the catch pan is allowed to preheat via the cone radiation for 1 min, while the sample is insulated by a thermal shield. This minimizes the pan's heat-sink effect when the flaming liquid starts dripping, so that a pool-fire is

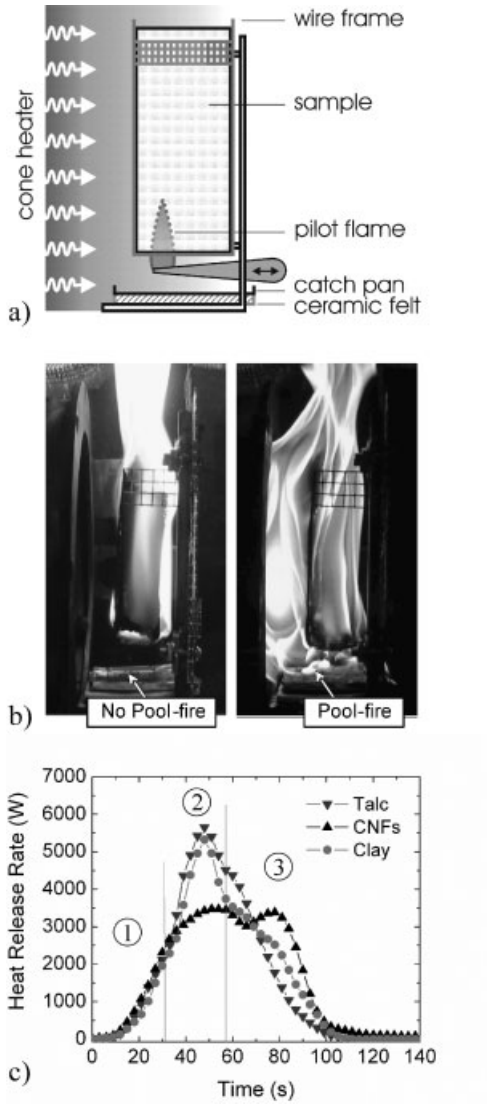

Figure 8. (a) Illustration of the apparatus used for the vertical cone calorimeter tests. (b) Carbon nanofiber foam (left) and talc foam (right) at the peak of heat release rate during the modified cone test. (c) Heat release rate from vertical cone calorimeter tests of the talc control sample, clay composite foam, and CNF composite foam. This figure is available in color online at www.interscience.wiley.com/journal/pat

rapidly formed. The external heat flux is set to 11 kW m^{-2} (measured on the vertical surface of the foam facing the cone) and a pilot flame (propane) impinges on the sample for 20 sec following the preheating phase. This test setup approximates a fire scenario where the foam is subjected mostly to the heat flux from the flame on the foam's surface; the low external heat flux imposed helps to establish stable flaming. The test is not intended to fully characterize the ignitability of the foam. Comparison with a newly developed test method (Vee-test) for medium sized foam slabs (300 mm × 600 mm × 75 mm) gave a correlation with an *r*-value of 0.97 for the peak of HRR of four commercially available foams measured with the small test presented here and the medium scale Vee-test.[21] This indicates that the results obtained here with the proposed modified cone test are meaningful in spite of the small size of the samples.

To evaluate the effectiveness of OMC and CNF as flame retardants in PUF composite foam, three foam formulations were compared using the new vertical cone calorimeter test: a talc control and the foams with OMC and CNFs. For each formulation a minimum of three replicates was tested. As previously mentioned, the three formulations had similar densities, but variations in airflow values are expected due to differences in cell structure. High density leads to a lower flame spread but the effect of airflow is still unclear.[22] Preliminary results show that the effect of airflow on the PHRR measured by our modified cone calorimeter is negligible.[23]

The heat release rate (HRR) of three representative samples is given in Fig. 8c. The talc and clay samples behaved very similarly, demonstrating the inability of the clay and talc additives, at the levels used here, to prevent melt dripping or to reduce HRR. These specimens went through three stages as indicated in Fig. 8c. In stage 1, the flame spreads over the surface, resulting in a molten front face of the specimen. In stage 2, droplets of flaming liquid fell on the catch pan giving rise to the formation of a pool-fire. The resulting increase in the burning surface area and the heat feedback between the pool-fire and the residual foam increase the HRR. The PHRR (peak in the heat release rate) is reached in the second half of stage 2, when the flow of molten material becomes very fast and the feedback is maximum; at this point the high HRR leads to a complete collapse of the foam. Finally, in stage 3, only the melt in the catch pan burns and the HRR decreases due to the lack of feedback and the decrease in burning surface area. In contrast, the CNF composite foam did not exhibit any melt flow to the catch pan. In addition, the sample retained its shape while only shrinking slightly. Fig. 8b shows an image of the CNF composite and the talc control burning at the time of the PHRR. The average PHRR for the CNF formulations is 3.68 ± 0.18 kW (σ); a reduction of 35% as compared to talc control (average PHRR 5.68 kW, ± 0.38 kW (σ)) is observed. This reduction in PHRR might be even higher in a real fire scenario, where the increase in the area of the pool-fire is not artificially limited as it is here by the catch pan dimensions.

The CNF foam produced a near-net-shape residue without dripping into the catch pan. Thus, it had a higher exposure to the external heat flux of the cone heater since the radiant flux from the cone is lower on the catch pan relative to that seen by the foam sample in the holder. In spite of this, the combustion performance was significantly improved for two main reasons: first, the flame generated by the pool-fire increased the total heat feedback to the talc and clay composites (Fig. 8b); second, an insulating residue (see Fig. 9) was formed on the surface of the CNF foam and shielded the underlying material. The total heat release is not significantly reduced by the CNF; the residue is 9% by mass for the formulation with CNF or talc, and 10% by mass for the OMC foam. The inorganic content for all three formulations is about 4% by mass, so some char is formed during combustion. As mentioned before, TGA data gave no increase in char yield both in air and in nitrogen. The CNF foam combustion produced a near-net-shape open-cell-foam structure (Fig. 9a). Due to the volatilization of the organic material, the CNF network shrank as the spaces between the fibers became voids. SEM analysis showed that

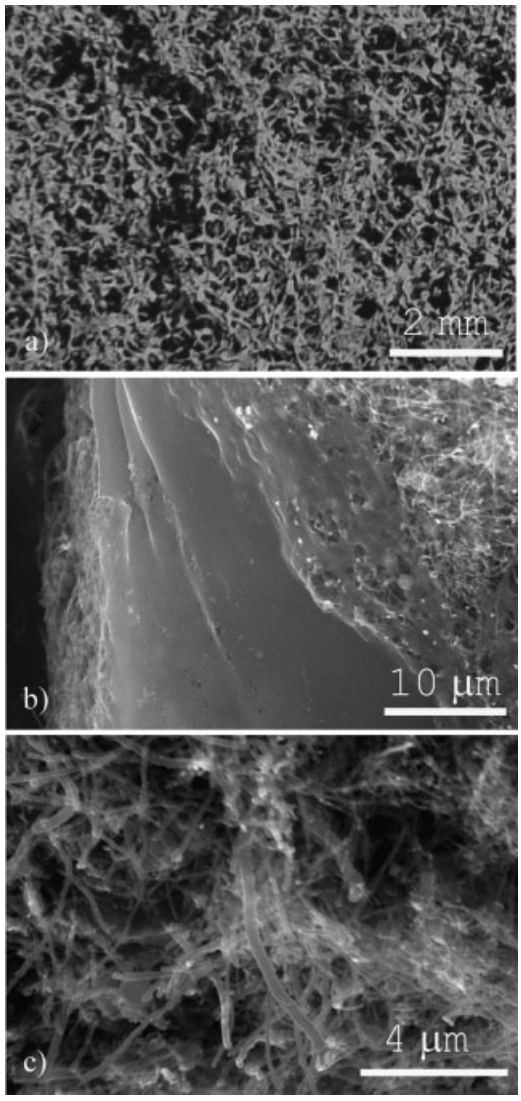

Figure 9. (a) Optical photograph of the burned residue from the CNF foam. CNFs in the foam retained their initial arrangement during the entire combustion process, forming an insulating near-net-shape structure with an extremely low density. (b) SEM micrograph showing the thin char layer. (c) SEM micrograph showing the entangled CNFs structure of the residue.

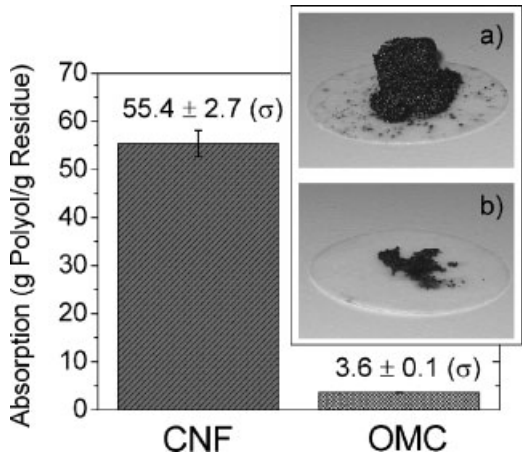

Figure 10. Polyol absorption capability measured on the residues from the modified cone test for: the CNF foam (CNF); the clay foam (OMC). The error bars (±σ) are shown. In the inset, the CNF (a) and the OMC (b) residues after polyol absorption are shown. This figure is available in color online at www.interscience.wiley.com/journal/pat

the char residue was composed of an entangled network of CNFs that retained their macroscopic arrangement during the combustion process (Fig. 9c). Presumably, the CNF network observed in the center of the foam struts (Fig. 3c) remained as a support during the combustion. The majority of the PUF resin volatilized although some formed the thin lamella-like char layers visible in the SEM of the residue (see Fig. 9b). This smooth char layer completely covers the underlying CNF network and it is a further clue that a biphasic core-skin structure is formed during foaming.

The polyol absorption on the residues from the modified cone test for CNF and clay foams was measured at a temperature of 80°C (Fig. 10). The CNF residue and OMC residue absorb an average of 55.4 $g_{polyol}/g_{residue}$ (where $g_{polyol}/g_{residue}$ is g of polyol per g of residue) and 3.6 $g_{polyol}/g_{residue}$, respectively. The CNF residue shows a sponge-like structure, able to absorb and retain a large amount of polyol. Taking into account that the residue from the CNF foam after the cone test is about 9% by mass, the amount of polyol that can be absorbed at 80°C is about 500 g per 100 g of foam. This is one order of magnitude larger than the theoretical amount of regenerated polyol produced by thermal degradation (about 59 g per 100 g of foam). This might explain the drip-free combustion of the CNF foam.

The contact angle values generated by the polyol in contact with OMC or CNF compressed film were $64^\circ \pm 2^\circ$ (σ) and $90^\circ \pm 2^\circ$ (σ), respectively (Fig. 11). The polyol wets the OMC surface (i.e. $\cos\theta > 0$), whereas no significant wetting is observed for the CNF surface (i.e. $\cos\theta \approx 0$).

Thus, wettability of the nanoparticle is not the key factor affecting polyol adsorption. According to the Jurin rule, the rise height h at the center of a circular capillary tube of small radius r immersed vertically in a large liquid bath is

$$h = \frac{2\gamma\cos\vartheta}{\rho g r} \quad (1)$$

where γ is the liquid-air surface tension, θ the contact angle, ρ the density of the liquid, g is the gravitational constant, and r is the radius of the tube.[24] It follows that the amount of polyol absorbed on CNFs by capillarity, according to Equation (1), should be negligible.

This result seems to contradict the high absorption values observed for the CNF residue. However, the contact angle measured here for a CNF compressed film might be significantly different from that measured on the CNF residue which also contains thin lamellar-like char layers (Fig. 9b). Furthermore, the adsorption in micropores (like those formed by the entangled CNFs, Fig. 9c) is dramatically different and generally larger from that described for a relatively wide capillary tube.[25]

Two elements appear to be crucial for the drip-free combustion of the CNF foam. First, the CNFs must be sufficiently entangled to retain the original network structure without collapse of the thin struts. Second, the liquid phase must be retained by the porous CNF network, rather than flow downward under the influence of gravity to

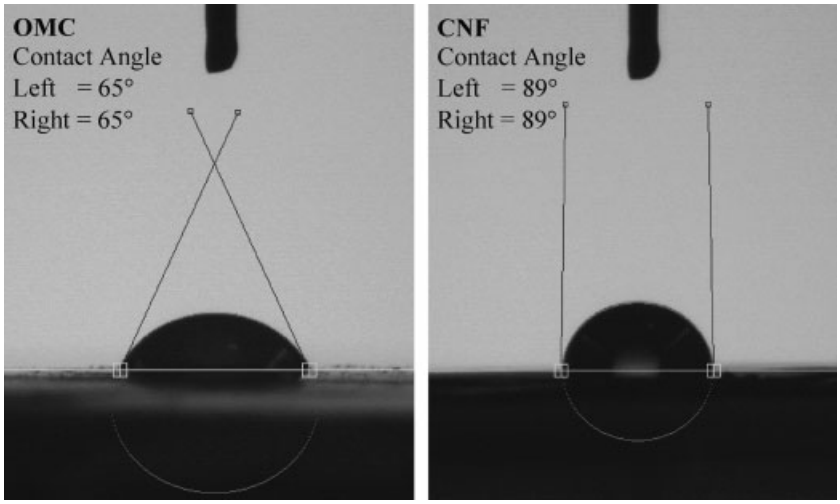

Figure 11. Contact angle between the polyol and a CNF or clay compressed film. This figure is available in color online at www.interscience.wiley.com/journal/pat

form individual droplets and subsequently a pool-fire. As shown in Fig. 3b, clays are also able to create a continuous network throughout the foam. However, particle–particle interactions and, in particular, entanglement are much higher for CNFs (aspect ratio $\rho = 200$–1700) as compared to clay ($\rho_{MAX} = 200$) due to the difference in aspect ratio and lack of exfoliation of the clay; this is most likely the reason why only CNFs generate a thermally stable network.

Hence, the presence of a thermally stable entangled fiber network and absorption by this network of the liquefied polymer are believed to be the key elements that prevent melt dripping of the CNF foams.

CONCLUSIONS

CNFs in PUFs, at a concentration of 4% by mass, give formation to a biphasic percolated system that appears to be critical to decreasing the fire hazard posed by PUFs by avoiding melt dripping and pool-fire formation. Flame spread is reduced by preventing the transfer of burning material to adjacent surfaces. HRR is lowered by removing flame feedback and reducing the burning surface area. CNFs in polyol induce a solid-like behavior that is thermally activated during the exothermic foaming process and/or thermal degradation. The formation of a biphasic core-skin structure in the strut increases the amount of CNFs in the core and reduces the critical concentration of nanoparticles required for a jammed network formation. The same core-skin effect and network formation is achieved with 5% by mass of intercalated OMC but, at this level, the clay network collapses during combustion and OMC is not effective at lowering the peak HRR or in stopping the melt dripping. The presence of a thermally stable entangled fiber network with high absorption capabilities is believed to be the key factor that prevents melt dripping. The entangled network prevents collapse of the foam and gives rise to the formation of a low density near net shape residue that shields the underlying material from the incident heat flux.

Acknowledgments

We acknowledge the contribution of Derek L. Ho (Polymers Division, NIST) for providing SAXS data.

REFERENCES

1. Kashiwagi T, Du F, Douglas JF, Winey KI, Harris RH, Shields JR. Nanoparticle networks reduce the flammability of polymer nanocomposites. *Nature Mater.* 2005; **4**: 928–933.
2. Kashiwagi T, Harris RH, Zhang X, Briber RM, Cipriano BH, Raghavan SR, Awad WH, Shields JR. Flame retardant mechanism of polyamide 6–clay nanocomposites. *Polymer* 2004; **45**(3): 881–891.
3. Kashiwagi T, Grulke E, Hilding J, Groth K, Harris R, Butler K, Shields J, Kharchenko S, Douglas J. Thermal and flammability properties of polypropylene/carbon nanotube nanocomposites. *Polymer* 2004; **45**(12): 4227–4239.
4. Ho DL, Lin EK, Wang C, Jones RL, Wu WL, Barton SW. In preparation.
5. Taylor BN, Kuyatt CE. Guidelines for evaluating and expressing the uncertainty of NIST measurement results. *NIST Technical Note 1297* 1994.
6. Zammarano M, Franceschi M, Bellayer S, Gilman JW, Meriani S. Preparation and flame resistance properties of revolutionary self-extinguishing epoxy nanocomposites based on layered double hydroxides. *Polymer* 2005; **46**(22): 9314–9328.
7. Alexandre M, Dubois P. Polymer-layered silicate nanocomposites: preparation, properties and uses of a new class of materials. *Mater. Sci. Eng.* 2000; **28**: 1–63.
8. Mcclusky JV, Priester RD, O'Neill RE, Willkomm WR, Heaney MD, Capel MA. The use of FT-IR and dynamic SAXS to provide an improved understanding of the matrix formation and viscosity build of flexible polyurethane foams. *J. Cell. Plast.* 1994; **30**: 338–360.
9. Sethumadhavan GN, Nikolov AD, Wasan DT. Stability of liquid films containing monodisperse colloidal particles. *J. Colloid Interface Sci.* 2001; **240**(1): 105–112.
10. Denkov ND, Cooper P, Martin JY. Mechanisms of action of mixed solid-liquid antifoams. 1. Dynamics of foam film rupture. *Langmuir* 1999; **15**(24): 8514–8529.
11. Oertel G. *Polyurethane Handbook* (2nd edn). Hanser: München, 1993.
12. Levchik SV, Weil ED. Thermal decomposition, combustion and fire-retardancy of polyurethanes—a review of the recent literature. *Polym. Int.* 2004; **53**(11): 1585–1610.
13. Ravey M, Pearce E. Flexible polyurethane foam. I. Thermal decomposition of a polyether-based, water-blown commercial type of flexible polyurethane foam. *J. Appl. Polym. Sci.* 1997; **63**(1): 47–74.
14. Metzner AB. Rheology of suspensions in polymeric liquids. *J. Rheol.* 1985; **29**: 739–779.
15. Rahatekar SS, Koziol KK, Butler S, Elliott JA, Shaffer M, Mackley M, Windle AH. Optical microstructure and viscosity enhancement for an epoxy resin matrix containing multiwall carbon nanotubes. *J. Rheol.* 2006; **50**(5): 599–610.
16. Lewin M, Pearce EM, Levon K, Mey-Marom A, Zammarano M, Wilkie CA, Jang BN. Nanocomposites at elevated temperatures: migration and structural changes. *Polym. Adv. Technol.* 2006; **17**(4): 226–234.
17. Kharchenko SB, Douglas JF, Obrzut J, Grulke EA, Milger KB. Nature Mater. 2004; **3**: 564–568.
18. Won YY, Meeker SP, Trappe V, Weitz DA. Effect of temperature on carbon-black agglomeration in hydrocarbon liquid with adsorbed dispersant. *Langmuir* 2005; **21**: 924–932.
19. Lefebvre J, Le Bras M, Bastin B, Paleja R, Delobel R. Flexible polyurethane foams: flammability. *J. Fire Sci.* 2003; **21**(5): 343–367.
20. Vanspeybroeck R, Van Hees P, Vandevelde P. Combustion behaviour of fabric and polyurethane flexible foam mock-up combinations under cone calorimetry test conditions. *Fire Mater.* 1993; **17**(4): 155–172.
21. Ohlemiller T, Shields J. Aspects of the fire behavior of thermoplastic materials. *NIST Technical Note 1493,* 2007.
22. Lefebvre J, Bastin B, Le Bras M, Dusquesne S, Ritter C, Paleja R, Poutch F. Flame spread of flexible polyurethane foam: comprehensive study. *Polym. Test.* 2004; **23**(3): 281–290.
23. Zammarano M, Harris R Jr, Gilman JW. In preparation.
24. Kornevand KG, Neimark AV. Modeling of spontaneous penetration of viscoelastic fluids and biofluids into capillaries. *J. Colloid Interface Sci.* 2003; **262**(1): 253–262.
25. Rouduner E. *Nanoscopic Materials Size-dependent Phenomena*. The Royal Society for Chemistry: Cambridge, UK, 2006; 166–168.